Linear Mesostructures in DNA–Nanorod Self-Assembly

Stephanie Vial,[†,‡] Dmytro Nykypanchuk,[†] Kevin G. Yager,[†] Alexei V. Tkachenko,[†] and Oleg Gang[*,†]

[†]Center for Functional Nanomaterials, Brookhaven National Laboratory, Upton, New York 11973, United States, and [‡]International Iberian Nanotechnology Laboratory, Braga, Portugal

ABSTRACT The assembly of molecules and nanoscale objects into one-dimensional (1D) structures, such as fibers, tubules, and ribbons, typically results from anisotropic interactions of the constituents. Conversely, we found that a 1D structure can emerge *via* a very different mechanism, viz, the spontaneous symmetry breaking of underlying interparticle interactions during structure formation. For systems containing DNA-decorated nanoscale rods, this mechanism, driven by flexible DNA chains, results in the formation of 1D ladderlike mesoscale ribbons with a side-by-side rod arrangement. Detailed structural studies using electron microscopy and *in situ* small-angle X-ray scattering (SAXS), as well as analysis of assembly kinetics, reveal the role of collective DNA interactions in the formation of the linear structures. Moreover, the reversibility of DNA binding facilitates the development of hierarchical assemblies with time. We also observed similar linear structures of alternating rods and spheres, which implies that the discovered mechanism is generic for nanoscale objects interacting *via* flexible multiple linkers.

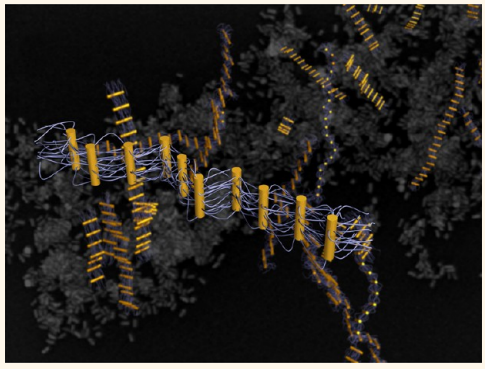

KEYWORDS: nanorods · DNA · self-assembly · assembly kinetics · mesostructure · symmetry breaking · one-dimensional structure

Breaking the perfect symmetry of a sphere in a simple way engenders a cylindrical object, i.e., a rod. This uniaxial anisotropy redefines the way that such objects can be organized in three dimensions, thus leading to a plethora of fascinating phenomena in the realms of liquid crystals, viruses, micro- and nanoparticles.[1−3] Typically, these systems exhibit a variety of liquid crystalline mesophases with partially broken symmetries, e.g., nematic and smectic. Such behavior, observed for a broad class of axially symmetric repulsive and attractive interactions between rods, is driven by a combination of entropic and enthalpic effects.[2,4,5] A departure from this common scenario has been observed in systems with strongly anisotropic interactions; for instance, the preferential attraction between the ends of rods results in a head-to-head binding and chainlike morphology.[6−8]

In this work, we report a qualitatively new assembly behavior in a system of rodlike nanoparticles wherein multiple DNA chains mediate interparticle interactions. The programmability of DNA and its polymeric nature recently were demonstrated as a powerful force in assembling bulk nanomaterials[9−11] and in the structural switching on demand.[12] For simple anisotropic particles (rods interacting *via* relatively rigid double-stranded (ds) DNA motifs) Jones et al. observed a morphology similar to that of traditional liquid crystalline systems with formation of a layered smectic B phase[13] as defined by the rod's anisotropy and interaction symmetry. Our findings show that for flexible molecular linkers, single-stranded (ss) DNA, a growth of 1D ladderlike ribbons of rods arranged side-by-side is the favored assembly pathway. Such unusual formation of 1D morphologies involves a spontaneous symmetry breaking of interactions between axially isotropic rods. As we will show, this behavior is due to collective effects associated with a flexibility of DNA linkers. The phenomenon is relevant to broad classes of nanoparticles interacting *via* polymer chains for which a rich structural diversity is expected.[14] The same mechanism also applies to the system of rods and spheres where it results in a linear morphology of alternating nano-objects. The reversibility of DNA hybridization affords the temporal

* Address correspondence to ogang@bnl.gov.

Received for review March 21, 2013 and accepted May 7, 2013.

Published online May 07, 2013
10.1021/nn401413b

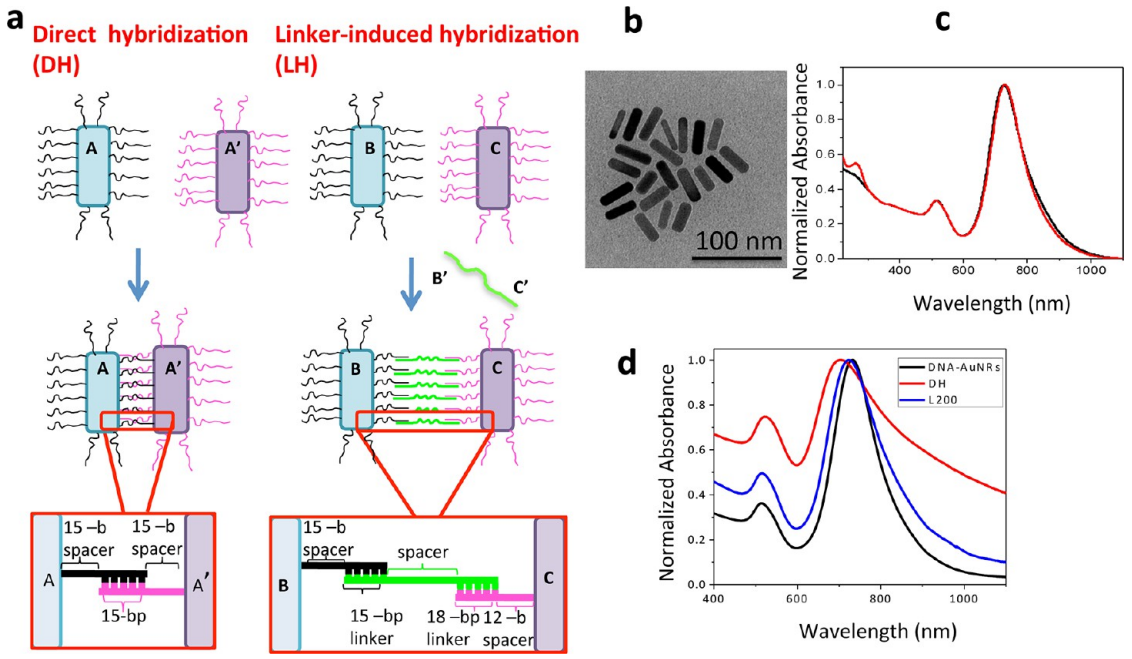

Figure 1. (a). Schematic of a gold nanorods (NR) assembly generated *via* direct or linker-induced DNA hybridization, and the detailed structure of one interparticle linkage. (b) TEM image of the NR. (c) UV−vis spectra of the as-synthesized NR (black) and DNA functionalized NR (red). (d) UV−vis spectrum of the NR before (black) assembly and after 24 h of assembly (red and blue lines correspond to DH and to L200, respectively).

evolution of 1D ribbons into 3D morphologies at the end of the assembly process. With the use of molecular blockers the evolution of the ribbon structure can be arrested, allowing the controllable formation of 1D nanoarchitectures.

RESULTS AND DISCUSSION

The binary systems studied in this work contain gold nanorods (NR) grafted with ssDNA providing Watson−Crick recognitions between rods (Figure 1a). Nanorods with an average length of 37 nm and a diameter $D \approx$ 9 nm (Figure 1b) were functionalized with one of four types of 30-base ssDNA (Figure 1c), denoted as A, A′, B, and C (Table S1 in Supporting Information), with A and A′ being complementary. This design facilitates the following self-assembly schemes (Figure 1a): (i) direct hybridization (DH), where assembly occurs *via* the hybridization of 15 complementary bases (A-A′ recognition of ssDNA attached to the NR) and (ii) linker-induced hybridization (LH), where B′ and C′ ssDNA ends, respectively, are complementary to B and C *via* 15- and 18-base recognition sequences, while B and C are mutually noncomplementary. We used ssDNA linkers (Table S2 in Supporting Information [SI]) with 33- (L33), 100- (L100) and 200-bases (L200) at the ratio of 200 per rod, i.e., below the surface-saturation limit.

Upon mixing complementary rods in the DH scheme or in the presence of the linker for the LH scheme, the rods begin to assemble, as evidenced by a change in the plasmon resonance bands measured by UV−vis spectroscopy (Figure 1d). The thermally reversible assembly/disassembly of aggregates (Figure S1 in SI) highlights the dominant role of hybridization in the assembly process. The low volume fraction ($<10^{-5}$) of the nanorods excludes the role of entropy in their orientation. The evolution of NR longitudinal (LP) and transverse (TP) surface plasmon bands[15] at 726 and 514 nm, respectively, provides qualitative information on the rods' alignment within the assembly. In particular, we observed a counter-directional shift of the LP and TP bands in UV−vis spectra, with relatively large, blue LP shifts of 32 and 13 nm, and smaller, red TP shifts of 7 and 1 nm, respectively, for DH and L200 systems after 24 h of assembly. Such changes indicate a predominantly side-by-side alignment[16] of the NR. At the same time, the decreased magnitude of the plasmon shift with DNA length signifies the reduced strength of plasmon coupling for larger rod−rod separations. At later stages of assembly (>24 h) 3D aggregation is evident from the red-shifts of the LP and TP bands in systems with shorter DNA, while the plasmon shifts are reduced for longer linkers (Figures S2 and S3 in SI).

To probe the structural details of the NR assemblies for different DNA motifs and the time evolution, we first applied scanning electron microscopy (SEM) (Figure 2). We have adopted a sample preparation procedure (see Methods) that preserves the in-solution assembly morphologies and minimizes artifacts caused by liquid flow and drying during the transfer from the solution to the air[17] by immobilizing nanorods on an oppositely charged substrate *via* electrostatic interactions.[18] Thus, we can collect and analyze the assemblies at different stages of the structure formation. Representative SEM images reveal the formation

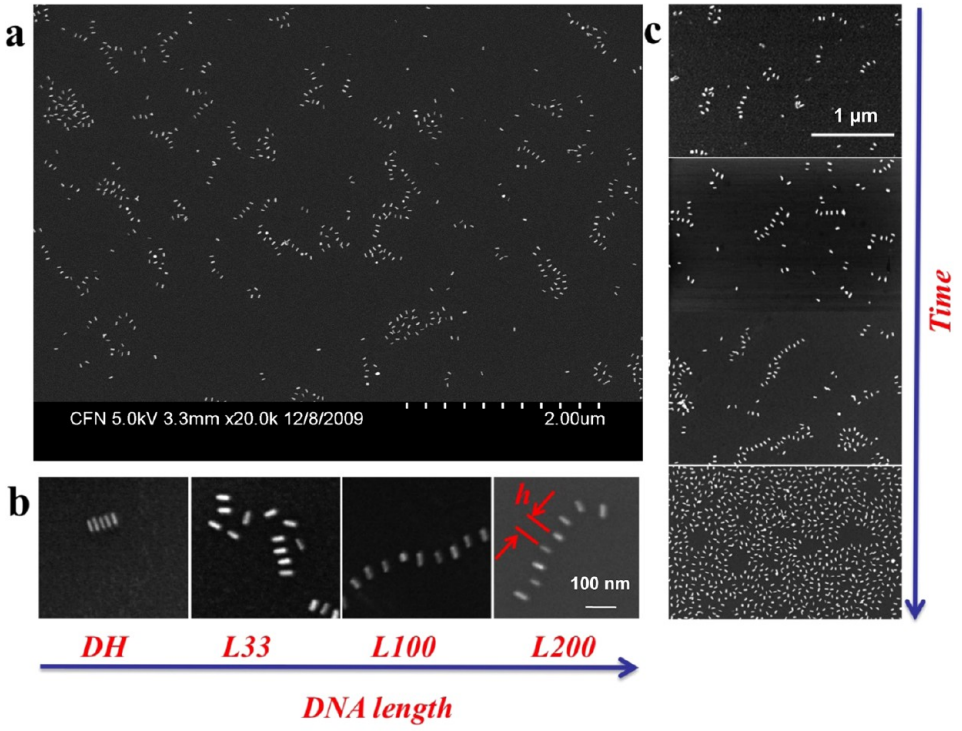

Figure 2. SEM images, obtained after collecting and washing assembled structures on positively charged substrates to preserve their morphology, as discussed in the text. (a) L200 NR system assembly in ribbon morphologies 8 h after assembly initiation. (b) The representative SEM images of ribbons for the DH, L33, L100, L200 systems show similar assembly morphologies, but different inter-rod distances, *h*, and ribbon flexibility, collected at 6 h of assembly. (c) The time evolution of assembly morphologies of NR for L200 system. The shown images correspond (from top to bottom) to 1, 3, 8, 24 h from assembly initiation, respectively.

of 1D ribbonlike structures with side-by-side rod arrangements after initiation of the assembly process (Figure 2), agreeing with our findings from UV−vis spectroscopy. No assembly was observed in our control experiments for noncomplementary NR (Figure S4c in SI). The inter-rod separations and the ribbon flexibility increase for longer DNA (Figure 2b), resulting in the average center-to-center distances, *h*, between rods of 23.5, 31.5, 45, and 61 nm for DH, L33, L100, and L200, respectively. The kinetics of assembly at this stage is faster for systems with longer DNA. The structures typically consist of only a few particles for the DH and L33 systems, whereas formation of well-developed ribbons is observed for the L100 and L200 systems (Figure S4 in SI). Monitoring the assembly process with time by SEM demonstrates the growth of ribbons (Figure 2c) without any noticeable change in inter-rod separation. After about 8 h of assembly we observe an appearance of larger aggregates that eventually reach micrometer sizes (Figure S4e in SI) at the assembly times ~24 h; ribbon structure can be resolved by SEM for the "skin" layer of the aggregates using the electrostatic deposition method discussed above (Figure S4f in SI). The structural details cannot be elucidated solely on the basis of SEM measurements since this method does not provide information of the in-solution behavior of NR assemblies. Therefore, we applied small-angle X-ray scattering (SAXS) to investigate assembly process and to obtain a quantitative measure of ensemble behavior.

We employed synchrotron-based *in situ* small-angle X-ray scattering (SAXS) to study the structural evolution of rod assemblies in solution (see Methods), Figures 3a and 4a. Figure 3a plots the development with time of the structure factors $S(q)$ for a representative example of rods linked with L100 (other systems are shown in Figures S5−7 in SI). The peaks in $S(q)$ typically emerge (Figure 3a) within 15 min of the onset of NR assembly. The positions of the higher-order diffraction peaks, q_n, scale approximately as multiples of the first peak position, q_1, suggesting a periodic 1D structure of finite size (see SI). This type of organization is consistent with ribbons of equidistantly placed rods, similar to those we observed by SEM. During up to 48 h of monitoring with SAXS, we noted a gradual increase of diffraction peak intensity, accompanied by an increase in the correlation length as indicated by narrowing of the peaks. At the same time, the internal structure of the ribbon evolves slightly during the growth, as is evident from a shift of q_1. Subsequently, beyond 48 h, we observed evidence of a new scattering peak, positioned at $q_s \approx 1.3q_1$, (Figure 3a). The absence of corresponding higher-order peaks suggests the lack of long-range order of that late-developed organization. The measured evolution of $S(q)$ revealed a similarity among the systems with longer DNA connections

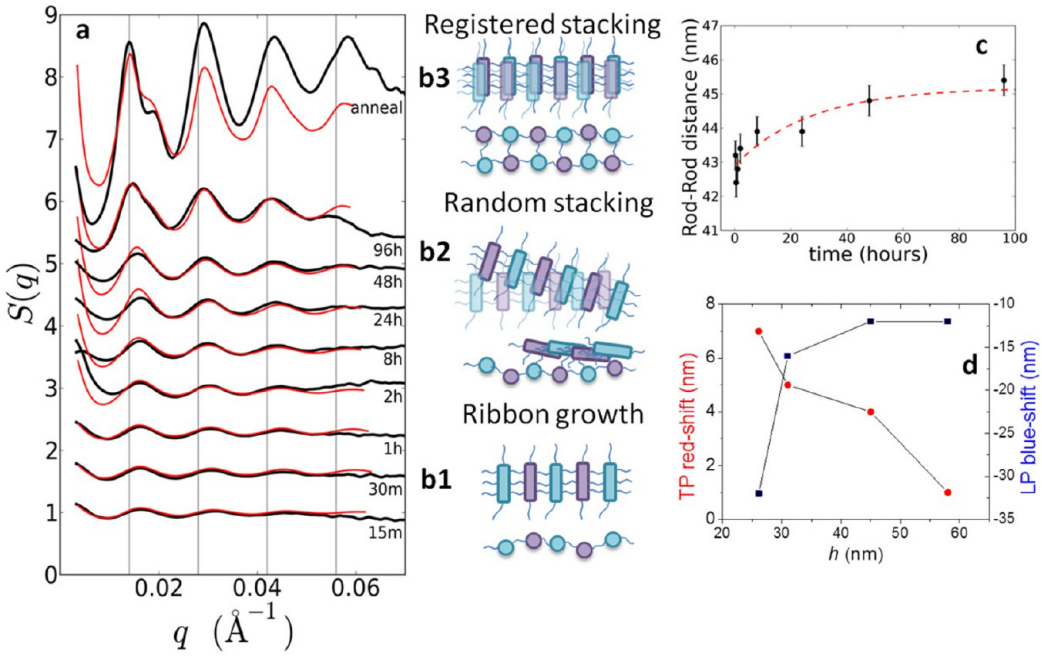

Figure 3. (a) Measured structure factors $S(q)$ for the NR system assembled with linker L100 (black curves) at different assembly times, as indicated, and after annealing (top curve). Red curves correspond to modeled $S(q)$ as described in the text and SI. (b) Illustration of assembly regimes deduced from the analysis of structure factors: ribbon growth (b1), random stacking of ribbons (b2), and stacking of ribbons with registry of complementary NR (b3). (c) Evolution of the inter-rod distance h *vs* time for the L100 system obtained from the data analysis as described; the dashed red line is to guide the eye only. (d) The blue-shift of LP and the red-shift of TP bands of formed ribbons relative to unassembled NRs as functions of inter-rod distances obtained from SAXS measurements.

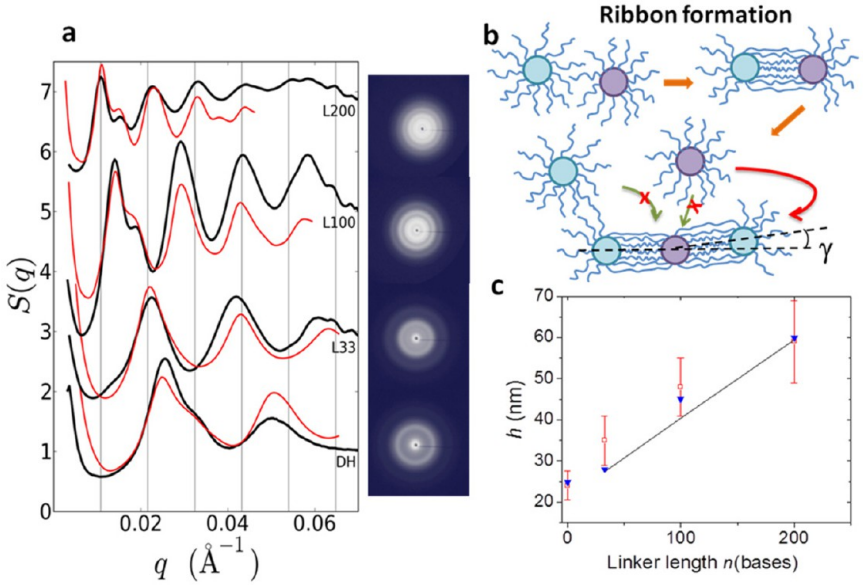

Figure 4. (a) SAXS images and extracted structure factors $S(q)$ for all studied systems after assembly and annealing at 37 °C for ~48 h and corresponding fits (red lines) as discussed in the text. (b) Schematic illustration (rod-end view) of the mechanism of spontaneous symmetry breaking engendering a ladderlike ribbon formation. (c) Evolution of the inter-rod distances obtained from SAXS (solid triangles) and SEM (open squares) measurements *vs* number of bases in a linker, with $n = 0$ corresponding to DH. The error bars are based on the standard deviation obtained from the SEM analysis (see the SI). The theoretical estimates for inter-rod distances, as discussed in the text, are shown with a solid line.

(L100 and L200), whereas in systems L33 and DH this behavior is less pronounced (see SI).

To uncover the details of assembled structures and their time evolution from SAXS data we quantitatively modeled the scattering of plausible morphologies (SI). We averaged the contributions of a large number of ribbons' lengths and configurations, thus accounting for their characteristics, i.e. length, flexibility, inter-rod bond length, and positional correlation within the ribbon. We note that for 1D organizations existing in

3D space, the correlation length measured by SAXS is influenced by a ribbon's length and its flexibility.[19] Our modeling (Figure 3a, red lines) allows delineating three regimes of ribbon development: ribbon growth, ribbon stacking, and registered stacking (Figure 3b). The early evolution of linked rods can be interpreted (Figures S8−9 in SI) as a growth of ribbons accompanied by increases of correlation length and interparticle distances (a and c in Figure 3). The inter-rod distances obtained by SAXS agree well with inter-rod distances observed with SEM (Figures 4c and S12−S15, S10a in SI). At 2 h assembly time, we detect a change in the ratio between peak positions from the predictions of a linear model, signifying a new assembly regime. Our model indicates a smeared electron density in the proximity of the ribbon, which can be attributed to a ribbon layering without mutual alignment (Figure 3b2), i.e. random ribbon stacking. The correlation length increase at this stage agrees well with this model, since the flexibility of a ribbon is constrained by neighbored ribbons. The SAXS measurements establish a relationship between inter-rod distance, h, and the shift of UV−vis spectroscopy measured plasmon bands relative to the free rods. In Figure 3d the blue-shift of the LP band and red-shift of the TP band are consistent with a side-by-side local arrangement of rods.

Finally, after >48 h assembly time, our analysis shows increasing alignment of ribbons, their stiffening (Figures S8 and S9 in SI), and their transition from a random stacking to short-range ribbon−ribbon registry (Figure 3b3) due to the rods complementarity, as signified by the appearance and increased intensity of the q_s peak. This stage can be viewed as a precursor to a square smectic B phase, a likely candidate for the ground state that satisfies a binary character of a system with DNA-encoded rods. Our analysis also indicates a slight increase (about 2 nm, Figure 3c) in the rod−rod distances for L100 during the structure evolution which can be attributed to the untangling of linkers and a consequent structure reorganization. A peak $q_s \approx 1.3q_1$, a signature of the local inter-ribbon ordering in a squarelike manner, appears for L200 and L100, whereas it is weaker for DH and not detectable for the L33 system (SI). These differences in the behavior of systems with DNA length are related to the role played by flexible chains, as we explain below. The annealing of the assembled systems for about 48 h results in the increased prominence of the q_s peak, especially for L200 and L100 (Figure 4a). Our modeling reveals that L200 exhibits even higher inter- and intra-ribbon correlations than L100, although both systems show a qualitatively similar behavior. In contrast, L33 and DH systems remain in the regime of random stacked and weakly connected ribbons (SI).

We interpret the observed assembly behavior by considering many-body effects that arise from the hybridization of multiple DNA chains between rods. For two interacting rods bound side-by-side with their ends in registry, the binding free energy, $E_2 = \varepsilon N$, is minimized when the number of DNA links, N, is maximized; here, ε includes DNA hybridization free energy, the elastic penalty for chain stretching, and the excluded volume contribution. When the third rod is added, its linkers will compete with those connecting the first two rods. Such a scenario applies only to sufficiently long, flexible DNA connections and effectively results in a nonadditive contribution to free energy, $E_3 = 2\varepsilon(N - \Delta_3)$. Here Δ_3 represents the number of DNA bonds between the first two rods which are broken due the newly formed connections to the third one. This parameter depends on the relative orientation of the two inter-rod bonds, i.e. angle γ in Figure 4b. The lowest overall free energy is expected when Δ_3 is minimal, which is realized for the two outer rods binding on the opposite sides of the middle one ($\gamma = 0$, Figure 4b). Binding the third neighbor to the same rod would require multiple DNA reconnections and therefore is kinetically suppressed, leading to linear growth. Our experiments indicate that this scenario can be fully realized for systems with longer DNA (L100 and L200) where chains are several times larger than the rod diameter D. On the other hand, the behavior is less pronounced when the two lengths are comparable (L33 and DH).

The collective chain behavior manifests through the linear dependence of inter-rod distance with the linker length (Figure 4c). Such dependence qualitatively differs from the well-known behavior of end-to-end chain distance and a scaling of a polymer brush thickness in a cylindrical geometry; it was not observed previously for ssDNA-assembled spheres.[11] In the connection region, each ssDNA chain is confined laterally within an effective tube due to the excluded volume interactions with other chains. This confinement causes DNA elongation, and the spacing between the rods can be expressed as

$$h = D + \frac{n_{ds}b_{ds}}{2} + \alpha n_{ss}b_{ss} \qquad \text{(eq 1)}$$

where n_{ds} and n_{ss} are numbers of bases in ds- and ssDNA segments, respectively, $b_{ds} \approx 0.35$ nm and $b_{ss} \approx 0.7$ nm are the corresponding separations of the bases along the DNA contour length. Parameter $\alpha < 1$ is the extension coefficient for ssDNA, defined as the ratio of its end-to-end distance to the contour length, $b_{ss}n_{ss}$.

Here we outline the theoretical model that allows one to calculate the extension of a single-stranded segment of the linkers in the system. For simplicity, we start with a planar geometry by considering two flat parallel surfaces connected with ssDNA linkers.

For this system, extension coefficient α can be determined from the condition that osmotic pressure $\Pi(\phi)$ is balanced by the elastic stress associated with the stretching of the chains:

$$\Pi(\phi) = \frac{1}{S}\frac{\partial}{\partial h}\left(\frac{3kTh_{ss}^2}{2an_{ss}b_{ss}}\right) = \frac{3kT}{aS}\frac{h_{ss}}{n_{ss}b_{ss}} \qquad \text{(eq 2)}$$

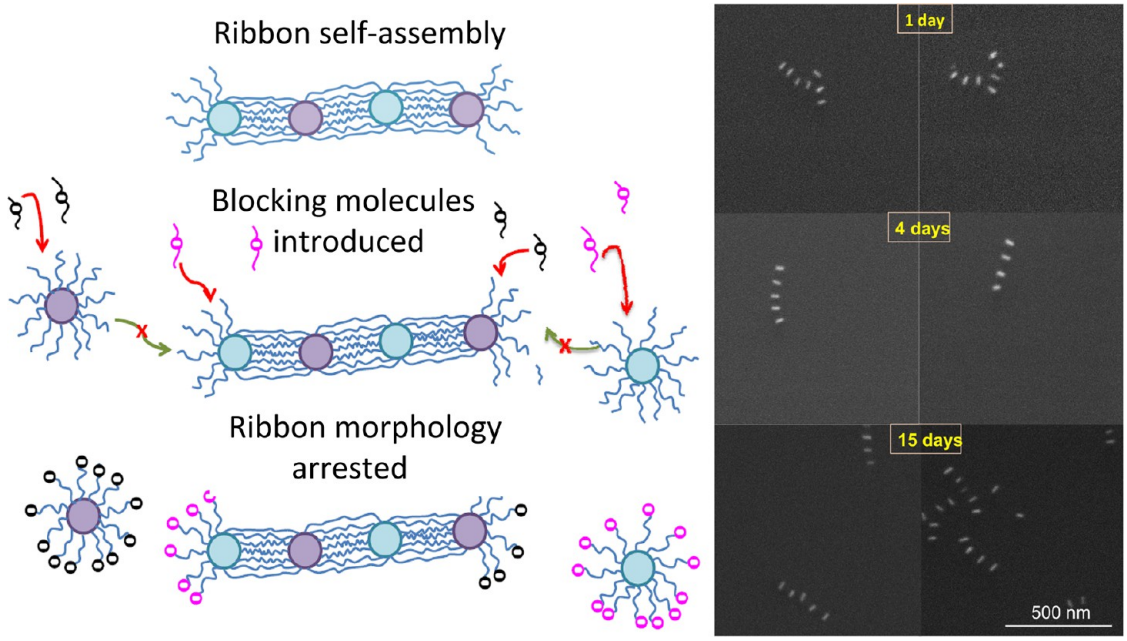

Figure 5. (Right) Self-assembly of rods in a ribbon morphology is stopped *via* introduction of blockers at the stage of assembly when ribbons have formed but did not start interacting significantly with each other. The blocking DNA strands, BS1 and BS2 (see Figure S16a and Table S3 in SI), hybridize with DNA attached to the rods, thus reducing a ribbon reactivity and leading to the arrest of ribbon growth and the reduction of inter-ribbon interactions (bottom). (Left) SEM images of nanorods with blocking sequences (excess 60) after 1, 4, and 15 days at 16 °C.

Here h_{ss} is the separation between the surfaces, S is the typical area per linker molecule, and we use the Gaussian model for chain elasticity, with the Kuhn segment of ssDNA $a \simeq 2$ nm.

Volume fraction of ssDNA can be expressed as $\phi = S_0 n_{ss} b_{ss}/(S h_{ss})$, where S_0 is the cross-sectional area of ssDNA. Therefore,

$$\alpha \equiv \frac{h_{ss}}{n_{ss} b_{ss}} = \left(\frac{S_0}{S}\right)\phi^{-1} \qquad \text{(eq 3)}$$

We now can combine the above two equations:

$$\left(\frac{S_0}{S}\right)^2 = \frac{a S_0 \phi \Pi(\phi)}{3kT} \qquad \text{(eq 4)}$$

This relationship allows us to find the equilibrium volume fraction ϕ, for a given linker coverage, and known dependence for $\Pi(\phi)$. The classical self-avoiding chain model for ssDNA predicts $\Pi(\phi) \simeq (kT/S_0 a)\phi^{\nu}$, ($\nu \simeq 9/4$). This yields $\phi \simeq (S_0/S)^{2/(\nu+1)}$, and therefore,

$$\alpha = \left(\frac{S_0}{S}\right)\phi^{-1} \simeq \left(\frac{S_0}{S}\right)^{\nu - 1/\nu + 1} \simeq \left(\frac{S_0}{S}\right)^{5/13} \qquad \text{(eq 5)}$$

In order to modify this calculation, to take into account curvature of the linked cylinders, one needs to account for spatial variation of both volume fraction and extension coefficient. Namely, the chains closer to the periphery are expected to be stronger stretched, and the middle region must have an osmotic pressure excess. The importance of this effect can be evaluated by noting that relative variation of the stretching coefficient across the system, $\delta\alpha/\alpha \simeq D/\alpha n_{ss} b_{ss}$, vanishes for long ssDNA. The corrections due to the curved geometry, and the corresponding deviation from the predicted linear scaling might be expected in the regime of short chains, $n_{ss} \lesssim D/\alpha b_{ss} \approx 30$.

Using this approach the best fit yields $\alpha \approx 0.3$ (Figure 4c) corresponding to experimentally relevant area per DNA linker, $S \simeq 10 nm^2$. Our model predicts α to be essentially independent of the chain length, thus, leading to a linear scaling of inter-rod distances, as observed experimentally (Figure 4c).

Two well-separated time scales required for the formation of ribbons from rods, and superstructures from ribbons result in the hierarchical assembly. The rearrangement of DNA connections drives the transition from a 1D ribbon assembly to locally registered stacking (b1−b3 of Figure 3). This evolution suggests that the ground state of the system is smectic B with in-plane square packing. However, we note that a small persistence length (∼1−2 nm) of ssDNA linkers precludes the formation of long-range square order; thus, only local squarelike inter-ribbon registration is observed. In the light of our model, that phase is preferred because one can reduce the free energy penalty (associated with DNA stretching that contributes to parameter ε) without sacrificing the total number of DNA connections. The observed slow kinetics of ribbon−ribbon assembly reflects the saturation of DNA bonds within the ribbon and the complexity of DNA `rewiring' required for creating multiple inter-ribbon links. The hierarchic nature of assembly is supported by observation that the

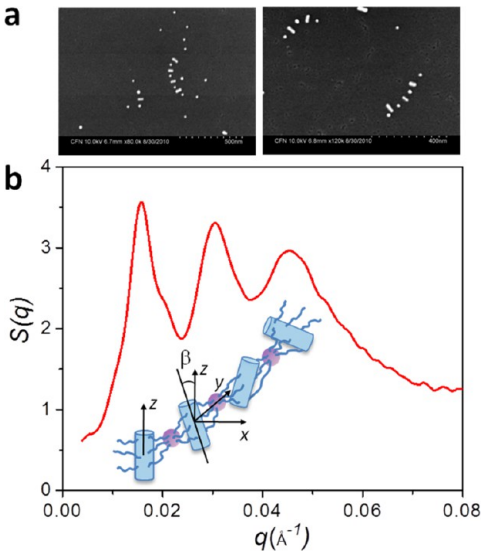

Figure 6. (a) SEM image of DNA functionalized rods and spheres assembled with DNA linker L100 in the ribbon with alternating placements of shaped particles. (b) $S(q)$ for the system shown in a. Schematic illustration of ribbon with alternating placement of rods and spheres without orientation of rods (inset). The angle β between the adjacent rods (orientated within the plane perpendicular to a ribbon axis) is random due to the symmetry of the rod−sphere bonds.

inter-ribbon links melt before intra-ribbon dehybridization occurs (Figure S1 in SI).

We took advantage of these two well-separated time assembly scales for individual ribbons and ribbons stacking, respectively, to arrest the assembly process in the stage of ladderlike ribbons. Our approach (Figure 5 and Figure S16a in SI) relies on the introduction of blocking ssDNA strands (Table S3 in SI) after ribbons have developed but while inter-ribbon interactions were still negligible. Blocking strands efficiently hybridize with DNA terminations that strongly suppress their reactivity with complementary NR. The process prevents inter-ribbon interactions and the consequent development of multiribbon superstructures. As result, the assembly population is arrested in the ribbon morphology, which is manifested by domination of ladderlike ribbons (Figure 5, left panel). Control experiments shown in Figure S16b (in SI) indicate no inter-ribbon stacking and rods aggregation for 15 days of observation. This approach can be potentially applied for a fabrication of linear structures with engineered plasmonic and fluorescent properties.

Remarkably, we also noted symmetry breaking when we substituted one type of rod with DNA-coated gold spheres of a similar diameter, 10 nm. SEM revealed the formation of ribbons in which rods and spheres alternate when hybridized with L100 (Figure 6a). SAXS measurements (Figure 6b) show an $S(q)$ pattern analogous to rod−rod systems, thus confirming the 1D character of this organization. This morphology can be understood within the proposed mechanism (Figure 4b). On the other hand, the intensity distribution of the $S(q)$ peaks showed no enhanced modulation corresponding to rod−rod periodicity, thereby implying an absence of orientational order for rods within ribbons (β is random, Figure 6b, inset), consistent with the rotational symmetry of rod−sphere interactions. The presence of common peak $q_s \approx 1.3q_1$ is indicative of stacking between ribbons, analogously to the discussed ribbons of rods, and it is realized in this system due to complementarity of rods and spheres from neighboring ribbons.

CONCLUSIONS

In summary, we observed a remarkable self-assembly behavior for DNA-decorated nanorods forming 1D ladderlike ribbons. This type of organization breaks the underlying axial symmetry of the rod−rod interactions, making it qualitatively different from chainlike structures with head-to-head arrangements.[6,8,20,21] Our proposed mechanism for this structural formation is attributed to multiple inter-rod bindings of flexible DNA linkers, and their competition for the binding spots. At a later assembly stage, ladderlike ribbons evolve toward a registered stacking organization, due to the formation of DNA bridges between ribbons. The 1D ribbon growth, followed by ribbons assembly, represents a hierarchic kinetic pathway *via* metastable states toward the ground state, which could be further exploited for nanofabrication. The observed scenario is reminiscent of self-assembly in biological systems, wherein molecules and supra-molecular complexes exhibit a hierarchy of primary, secondary, and higher-order structures formed at multiple time- and length-scales due to the complex energy landscape. The observed emergence of lower dimensional structures for homogeneously functionalized objects manifests a rich behavior of polymer-grafted colloids.[7,22,23] Recently, such formation of ladderlike structures from polymer-interacting rods was observed in computational studies.[25] Thus, the NR ribbons can be viewed as a generic class of structures with spontaneously reduced dimensionality.

METHODS

Nanorods Synthesis. We synthesized the gold nanorods by the seed-mediated method.[24] First, a gold seed solution was prepared by the borohydride reduction of 0.25 mM $HAuCl_4$ in an aqueous 0.1 M CTAB solution. Subsequently, the seed solution was added to a growth solution containing 0.1 M CTAB, 0.5 mM $HAuCl_4$, 0.06 mM silver nitrate, and 0.7 mM ascorbic acid. The solution was aged for 24 h to ensure the complete formation of NR. This protocol gives CTAB- stabilized gold nanorods, 37 nm long, with average diameter around 9 nm.

Nanoparticle Modification with DNA. Single-stranded thiolated-DNAs were immobilized on the surface of rods through S−Au bonds. Thiol-functionalized single-stranded oligonucleotides were purchased from IDT Inc. In a typical experiment, the samples were reduced by dissolving the lyophilized oligonucleotides (200−300 nmoles) in 0.3 mL of 100 mM dithiothreitol (DTT) solution in purified water or buffer, followed by 30 min incubation. The samples then were loaded on to a freshly purified sephadex column (NAP-5,GE Healthcare), and eluted with 2.5 mL 10 mM phosphate buffer (pH = 7.4). The DNA was quantified by UV−vis spectrometry. The synthesized NR were functionalized with DNA. In a typical experiment, an aliquot (200−300 μL) of 10−20 μM purified DNA solution was added to 1 mL of a purified water solution of NR (~2 nM), and the mixture incubated in an unbuffered solution for at least 12 h. To avoid the aggregation of nanorods, while adding the buffer and salt, we also incorporated sodium dodecylsulfate to a final concentration of 10 μM. Then, the mixture was brought to 10 mM concentration of phosphate buffer (pH = 7.4), and left for 1 h at room temperature. Afterward, the salt concentration was increased to 0.01 M of NaCl, and sample incubated for ~6 h; thereafter, more salt was added, bringing the NaCl concentration to 0.1 M, and the samples incubated for 12 h . The DNA-NR were stable for at least 2 weeks at this salt concentration. The solution was freed of excess DNA by three consecutive centrifugations at 8000 rcf for 30 min and supernatant exchange.

DNA−NR Assemblies. Particle assembly was carried out by combining equimolar amounts ([NR] ≃ 4 nM) of type-A and type-A′ or type-B and type-C DNA-capped gold particles with corresponding DNA linkers in 200 μL of a solution of 10 mM phosphate buffer, 0.1 M NaCl, pH = 7.4. For SAXS measurements, the solutions were transferred into 1-mm diameter quartz capillaries (Charles Supper, MA).

Transfer of Assembled Nanorods to Substrate for SEM Imaging. Silicon wafers were used as substrates. They were cleaned by sonication in a 1% solution of Alconox (Alconox Inc., NY), then in deionized water for 15 min, followed by a piranha solution. Afterward, the substrates were rinsed with copious amounts of deionized water and dried under a nitrogen stream. The clean substrates first were immersed in an aqueous solution of positively charged poly(diallyldimethylammonium chloride) (PDDA) (1 mg/mL in 0.5 M NaCl, M_w 10,000) for 30 min, then in an aqueous solution of polyanion poly(styrenesulphonate) (1 mg/mL in 0.5 M NaCl, M_w 15,000) for 10 min, and finally in the PDDA solution for 10 min. At this stage, the wafers are positively charged, favoring electrostatic interactions with negatively charged DNA−NR. To deposit nanorods on the substrates, we covered them with 100 μL of diluted DNA−NR dispersion (0.04 nM NR), incubated them for 1 h, rinsed them with deionized water, and finally dried them in a gentle stream of nitrogen.

Characterization. SAXS experiments were performed at the National Synchrotron Light Source's X9 beamline. The scattering data were collected with a charge-coupled device (CCD) area detector. The data are presented as the structure factor $S(q)$ *vs* scattering vector, $q = (4\pi/\lambda)\sin(\theta/2)$, where θ is the scattering angle. The values of q were calibrated with silver behenate (q_1 = 0.1076 Å^{-1}). $S(q)$ was calculated as $I_a(q)/I_p(q)$,[9,11] where $I_a(q)$ and $I_p(q)$ are the background-corrected angular-averaged one-dimensional scattering intensities for the system under investigation and the unaggregated system, respectively. The peak positions in S(q) were determined by fitting a Lorentzian function.

Ultraviolet−visible spectra were collected on a PerkinElmer Lambda 35 spectrometer with a temperature-controlled sample holder.

Scanning electron microscopy (SEM) images were obtained on a Hitachi 4800 scanning electron microscope.

Conflict of Interest: The authors declare no competing financial interest.

Acknowledgment. Research was carried out at the Center for Functional Nanomaterials, Brookhaven National Laboratory, which is supported by the U.S. Department of Energy, Office of Basic Energy Sciences, under Contract No. DE-AC02-98CH10886. O.G. acknowledges support by the U.S. Department of Energy, Basic Energy Sciences, Materials Sciences and Engineering Division. S.V. acknowledges financial support from International Iberian Nanotechnology Laboratory (INL) in Braga, Portugal.

Supporting Information Available: The sample preparation procedure, structure details, and optical properties of NR assemblies; SAXS modeling and structural data analysis; analysis of SEM data; and the description of the process for the NR assembly arresting in the ladderlike ribbons. This material is available free of charge via the Internet at http://pubs.acs.org.

REFERENCES AND NOTES

1. Dogic, Z.; Fraden, S. Ordered Phases of Filamentous Viruses. *Curr. Opin. Colloid Interface Sci.* **2006**, *11*, 47–55.
2. Baranov, D.; Fiore, A.; Huis, M.; Van Giannini, C.; Falqui, A.; Lafont, U.; Zandbergen, H.; Zanella, M.; Cingolani, R.; Manna, L. Assembly of Colloidal Semiconductor Nanorods in Solution by Depletion Attraction. *Nano Lett.* **2010**, *10*, 743–749.
3. Barry, E.; Dogic, Z. Entropy Driven Self-Assembly of Nonamphiphilic Colloidal Membranes. *Proc. Natl. Acad. Sci. U.S.A.* **2010**, *107*, 10348–10353.
4. Dujardin, E.; Mann, S.; Hsin, L.-B.; Wang, C. R. C.; Mann, S. DNA-driven Self-Assembly of Gold Nanorods. *Chem. Commun.* **2001**, 1264–1265.
5. Liu, Q.; Cui, Y.; Gardner, D.; Li, X.; He, S.; Smalyukh, I. I. Self-Alignment of Plasmonic Gold Nanorods in Reconfigurable Anisotropic Fluids for Tunable Bulk Metamaterial Applications. *Nano Lett.* **2010**, *10*, 1347–1353.
6. Caswell, K. K.; Wilson, J. N.; Bunz, U. H. F.; Murphy, C. J. Preferential End-to-End Assembly of Gold Nanorods by Biotin−Streptavidin Connectors. *J. Am. Chem. Soc.* **2003**, *125*, 13914–13915.
7. Liu, K.; Nie, Z.; Zhao, N.; Li, W.; Rubinstein, M.; Kumacheva, E. Step-Growth Polymerization of Inorganic Nanoparticles. *Science* **2010**, *329*, 197–200.
8. Walker, D. A.; Gupta, V. K. Reversible End-to-End Assembly of Gold Nanorods Using a Disulfide-modified Polypeptide. *Nanotechnology* **2008**, *19*, 435603.
9. Nykypanchuk, D.; Maye, M. M.; van der Lelie, D.; Gang, O. DNA-guided Crystallization of Colloidal Nanoparticles. *Nature* **2008**, *451*, 549–552.
10. Park, S. Y.; Lytton-Jean, A. K. R.; Lee, B.; Weigand, S.; Schatz, G. C.; Mirkin, C. A. DNA-Programmable Nanoparticle Crystallization. *Nature* **2008**, *451*, 553–556.
11. Xiong, H.; van der Lelie, D.; Gang, O. Phase Behavior of Nanoparticles Assembled by DNA Linkers. *Phys. Rev. Lett.* **2009**, *102*, 015504.
12. Maye, M. M.; Kumara, M. T.; Nykypanchuk, D.; Sherman, W. B.; Gang, O. Switching Binary States of Nanoparticle Superlattices and Dimer Clusters by DNA Strands. *Nat. Nanotechnol.* **2010**, *5*, 116–120.
13. Jones, M. R.; Macfarlane, R. J.; Lee, B.; Zhang, J.; Young, K. L.; Senesi, A. J.; Mirkin, C. A. DNA-Nanoparticle Superlattices Formed from Anisotropic Building Blocks. *Nat. Mater.* **2010**, *9*, 913–917.
14. Chremos, A.; Panagiotopoulos, A. Structural Transitions of Solvent-Free Oligomer-grafted Nanoparticles. *Phys. Rev. Lett.* **2011**, *107*, 1–5.
15. Perez-Juste, J.; Pastoriza-Santos, I.; Liz-Marzan, L. M.; Mulvaney, P. Gold Nanorods: Synthesis, Characterization and Applications. *Coord. Chem. Rev.* **2005**, *249*, 1870–1901.
16. Jain, P. K.; Eustis, S.; El-Sayed, M. A. Plasmon Coupling in Nanorod Assemblies: Optical Absorption, Discrete Dipole Approximation Simulation, and Exciton-Coupling Model. *J. Phys. Chem B* **2006**, *110*, 18243–18253.
17. Oliver, S. R. J.; Bowden, N.; Whitesides, G. M. Self-Assembly of Hexagonal Rod Arrays Based on Capillary Forces. *J. Colloid Interface Sci.* **2000**, *224*, 425–428.
18. Vial, S.; Pastoriza-Santos, I.; Pérez-Juste, J.; Liz-Marzan, L. M. Plasmon Coupling in Layer-by-Layer Assembled Gold Nanorod Films. *Langmuir* **2007**, *23*, 4606–4611.
19. Roe, R.-J. *Methods of X-ray and Neutron Scattering in Polymer Science*; Oxford University Press: New York, 2000; p 360.

20. Huang, H.; Liu, X.; Hu, T.; Chu, P. K. Ultra-Sensitive Detection of Cysteine by Gold Nanorod Assembly. *Biosens. Bioelectron.* **2010**, *25*, 2078–2083.
21. Shibu Joseph, S. T.; Ipe, B. I.; Pramod, P.; Thomas, K. G. Gold Nanorods to Nanochains: Mechanistic Investigations on Their Longitudinal Assembly Using α,ω-Alkanedithiols and Interplasmon Coupling. *J. Phys. Chem. B* **2006**, *110*, 150–157.
22. Akcora, P.; Liu, H.; Kumar, S. K.; Moll, J.; Li, Y.; Benicewicz, B. C.; Schadler, L. S.; Acehan, D.; Panagiotopoulos, A. Z.; Pryamitsyn, V.; et al. Anisotropic Self-Assembly of Spherical Polymer-grafted Nanoparticles. *Nat. Mater.* **2009**, *8*, 354–359.
23. Jahn, S.; Geerts, N.; Eiser, E. DNA-mediated Two-Dimensional Colloidal Crystallization Above Different Attractive Surfaces. *Langmuir* **2010**, *26*, 16921–16927.
24. Nikoobakht, B.; El-Sayed, M. A. Preparation and Growth Mechanism of Gold Nanorods (NRs) Using Seed-mediated Growth Method. *Chem. Mater.* **2003**, *15*, 1957–1962.
25. Knorowski, C.; Travesset, A. Nanorods in Functionalized Block-Copolymer Gels: Flexible Ladders and Liquid Crystalline Order in Curved Geometries. *Europhys. Lett.* **2012**, *100*, 56004.